Lanthanide 4*f*-level location in lanthanide doped and cerium-lanthanide codoped NaLaF$_4$ by photo- and thermoluminescence

A. H. Krumpel,[1,a)] E. van der Kolk,[1] D. Zeelenberg,[1] A. J. J. Bos,[1] K. W. Krämer,[2] and P. Dorenbos[1]

[1]*Faculty of Applied Sciences, Delft University of Technology, Mekelweg 15, 2629 JB Delft, The Netherlands*
[2]*Department of Chemistry and Biochemistry, University of Bern, Freiestrasse 3, 3000 Bern 9, Switzerland*

Photo- and thermoluminescence (TL) spectra of NaLaF$_4$:Ln^{3+} (Ln=Ce,Pr,Nd,Sm,Eu, Gd,Tb,Dy,Ho,Er,Tm) and NaLaF$_4$:Ce^{3+}, Ln^{3+} (Ln=Nd,Sm,Ho,Er,Tm) are presented and used together with the empirical Dorenbos model in order to establish the 4f energy level positions of all tri- and divalent lanthanide ions doped in NaLaF$_4$. The information will be presented in the form of an energy level diagram. It is shown that in addition to this diagram only two assumptions, viz., the presence of two host related electron traps and the presence of V_k-centers, are necessary for explaining the lanthanide-specific TL glow curves of both Ln mono- and Ce–Ln codoped NaLaF$_4$. © 2008 American Institute of Physics. [DOI: 10.1063/1.2955776]

I. INTRODUCTION

Luminescence properties of lanthanide (Ln) doped phosphors depend strongly on the position of the excited 5d and the 4f levels, both relative to each other and to the electronic states of the host, i.e., the valence band (VB) and the conduction band (CB). Since a few years ago, an empirical model developed by Dorenbos has been available. It helps to set the 4f and 5d levels of all lanthanides in an inorganic compound once the position for only one of them is known. The objective of this study on Ln doped sodium lanthanum fluoride (NaLaF$_4$) was the localization of the di- and trivalent Ln 4f and 5d energy levels by photoluminescence (PL) and thermoluminescence (TL) studies.

The Dorenbos model[1] relies on the observations that for all lanthanides the energy difference between the lowest 5d energy levels and the top of the VB is approximately the same and that the energy of the first 4f-5d transition relative to that in the free Ln ions is lowered nearly by the same amount for all lanthanides. This indicates an almost equal interaction of the Ln 5d levels with the crystal field and effectuates an inversion of the almost host-invariant Dieke diagram in such a way that the variation over the Ln series in the energy difference between the Ln 4f ground state energy (GSE) and the top of the VB reveals independently from the host a characteristic double-seated shape.[2] Thus, knowledge about the absolute 4f GSE location for only one Ln ion suffices to set the GS of all other ions at the same time. Diverse theoretical attempts using band calculations and cluster models have been made in order to describe the role of the 4f electrons in chemical bonding and position 4f levels relative to the VB of a host.[3] Unfortunately, those calculations are difficult and labor-intensive. In contrast, the energy level scheme according to the Dorenbos model places the 4f and 5d energy levels of the lanthanides based on empirical laws and not on theoretical calculations. Despite its relative simplicity, it allows for predictions with a high degree of accuracy. Using the empirical model together with experimental information from vacuum ultraviolet (vuv) spectroscopy, an energy level scheme for NaLaF$_4$:Ce^{3+} (Ln =La,Ce,Pr,…,Lu) was constructed. Once such a scheme for NaLaF$_4$ was available, we were able to hypothesize how the Ln ions would behave under high energy irradiation. In NaLaF$_4$:Ce^{3+}, Ln^{3+}, for instance, the 4f GS of Ce^{3+} being energetically located several eV above the VB could trap a hole as proposed in Y$_2$SiO$_5$.[4,5] The GS of the second Ln dopant in the divalent form, in contrast, if chosen correctly with regard to the energy level diagram, could serve as an electron trap. By means of TL studies, we could verify this kind of hypothesis. The application of the Dorenbos model to TL in this work is an example for its easy, practical use and its possible value in the search of new materials of economic and technological interest.

II. EXPERIMENTAL

A. Sample preparation

Powder samples of phase-pure hexagonal NaLaF$_4$:2% RE^{3+} (RE=Ce,Pr,Nd,Sm,Eu,Gd,Tb,Dy,Ho,Er,Tm) fluorides were prepared from rare-earth oxides Re$_2$O$_3$ (Re =La,Ce,Pr,Nd,Sm,Eu,Gd,Tb,Dy,Ho,Er,Tm) of 5N or 6N purity (Metall Rare Earth Limited), Na$_2$CO$_3$ (Alfa, 5N), and aqueous 47% HBr and 40% HF acids (Merck, supra pure). Batches were typically calculated for 5 g of product. The stoichiometric mixture of the respective rare-earth oxides was dissolved in a small amount of HBr in a Teflon beaker, evaporated to dryness, dissolved in water, and the fluorides MF$_3$ precipitated with HF. The liquid is evaporated and HF is added again. The appropriate amount of Na$_2$CO$_3$ to obtain a 2:1 ratio of Na to *M* is dissolved in water in a separate beaker and slowly added to the mixture. Care has to be taken to avoid spilling due to the CO$_2$ evolution. The product is dried, and the addition of HF and drying are re-

a)Author to whom correspondence should be addressed. Tel.: +31-15-27-81954. FAX: +31-15-27-89011. Electronic mail: a.h.krumpel@tudelft.nl.

peated. The solid, which consists of a mixture of MF_3, NaF, and NaBr according to x-ray diffraction, is ground up in a mortar, transferred into a glassy carbon boat, and heated to 550 °C in a HF/Ar gas stream for 20 h. In this step, the reaction toward hexagonal $NaMF_4$ plus excess NaF takes place. Traces of O and Br are removed by the HF gas stream. The powder is ground up again and heated to 590 °C in an Ar gas stream for another 20 h. This step improves the crystallinity and optical properties of the material. Finally, the product is washed with water to dissolve the excess NaF and then dried at 100 °C. All samples were checked by x-ray powder diffraction. They show the hexagonal $NaLaF_4$ phase[6,7] together with a small residue of about 0.5% NaF. $NaLaF_4$ crystallizes in space group $P\bar{6}$ and has two La^{3+} sites, which are randomly occupied by the dopant ions. Both sites have tricapped trigonal prismatic coordination, one with C_{3h} and the other with C_1 site symmetry, respectively.[6] Since the lanthanides have the same valency and are of comparable size as the lanthanum ions in the $NaLaF_4$ host compound, a statistical distribution of dopant ions is assumed. They are not expected to cause large lattice distortions and defects. Therefore, we expect a minimal number of host related traps, which makes it easier to understand the nature of Ln-specific glow peaks.

B. Experimental techniques

All PL spectra were recorded at the Deutsches Elektronen-Synchrotron (DESY) in Hamburg (Germany) using the SUPERLUMI station of HASYLAB. For the excitation spectra, the spectral region of excitation was 50–335 nm with a fixed resolution of 0.3 nm. An R6358P Hamamatsu photomultiplier tube (PMT) connected to a triple grating Czerny–Turner monochromator SpectraPro-308i from Acton Research, Inc., was used to measure the luminescence from UV to visible wavelengths. All excitation spectra were corrected for the wavelength dependent excitation intensity.

The emission spectra were recorded with a liquid nitrogen cooled charge coupled device (CCD) detector (Princeton Instruments, Inc.) connected to the monochromator described above. The sensitive spectral range was between 200 and 1100 nm with a resolution close to 1 nm. All emission spectra were corrected for the wavelength dependent detection efficiency. All PL data presented were recorded at 10 K.

The TL measurements were done with a RISØ system (model TL/OSL-DA-15), consisting of an automated TL/OSL reader incorporated into a 386-based PC, a turntable with 48 sample positions, and a $^{90}Sr/^{90}Y$ beta source with a dose rate of 1 mGy s^{-1}. The TL glow curves from the Ln monodoped samples were recorded using a broadband filter with a transmission range of 320–660 nm and a full width at half maximum (FWHM) of 242 nm. For the glow curves from the Ce–Ln codoped samples, a filter with a transmission range of 280—380 nm and a FWHM of 70 nm was used. The Ce^{3+} emission is therefore recorded in these latter TL curves. The emitted light of each individually heated sample was detected by a PMT (model 9235QA, Electron Tubes Limited) or a CCD camera in case of the λT-contour plots. In the case of the λT-contour plots, the samples were
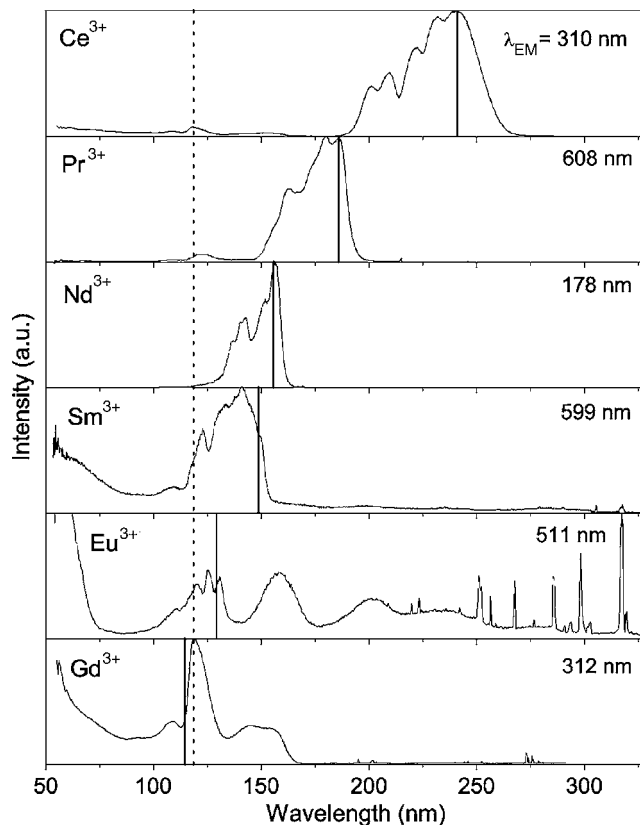

FIG. 1. Excitation spectra of $NaLaF_4:Ln^{3+}$ recorded at 10 K; Ln and emission wavelengths λ_{EM} are specified for each spectrum in the figure.

irradiated with an external ^{60}Co source with a dose rate of 4.06 kGy h^{-1}. All TL measurements were done in nitrogen atmosphere.

III. RESULTS

A. Photoluminescence

The excitation spectra of $NaLaF_4:Ln^{3+}$ (Ln=Ce, Pr, Nd, Sm, Eu, Gd) are shown in Fig. 1. They were recorded at 10 K. All excitation spectra have a band around 119 nm (accentuated by the dotted line) and a second band at slightly higher energies. $NaLaF_4:Eu^{3+}$ reveals very clearly the fluoride-europium charge transfer (CT) band around 160 nm; the broad bands between 170 and 300 nm are assigned to CT involving oxygen impurities. Both $NaLaF_4:Ce^{3+}$ and $NaLaF_4:Gd^{3+}$ show broad bands around 150 nm, which could not be identified. In Fig. 1 also the lowest 4f-5d transitions are indicated by vertical lines showing a clear trend to higher energies going from cerium to gadolinium.

Figure 2 shows the emission spectra for $NaLaF_4:Ln^{3+}$ (Ln=Ce, Pr, Nd, Sm, Eu, Gd) recorded at 10 K. The emission energies are summarized in Table I and attributed to the respective 4f-4f and 5d-4f transitions. The range of the 4f-4f transition energies is given by the Stark components of the corresponding 2J+1 degenerate initial and terminal multiplets. The 5d-4f transitions are relatively high in energy as fluorides tend to have the smallest spectroscopic redshift of all inorganic compounds.[8,9] $NaLaF_4:Ce^{3+}$ shows under 240 nm excitation the two $5d^1 \rightarrow 4f^1:{}^2F_j$ ($J=5/2, 7/2$) emissions as two unresolved bands with a peak at 300 nm
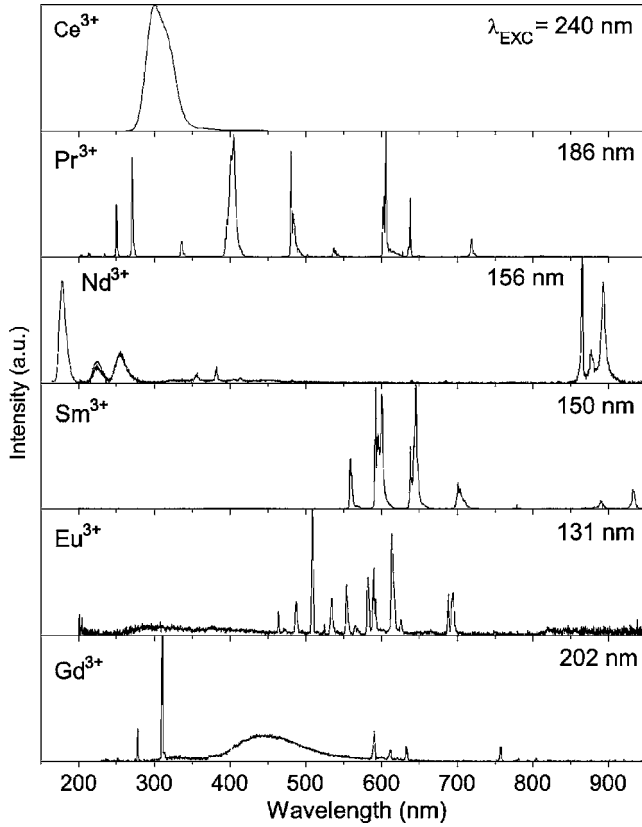
FIG. 2. Emission spectra of NaLaF$_4$:Ln^{3+} recorded at 10 K; Ln and excitation wavelengths λ_{EXC} are specified for each spectrum in the figure.

TABLE I. Emission lines and corresponding multiplet transitions for the light Ln dopant ions.

Ln^{3+}	Transition	Energy ($\times 10^3$ cm^{-1})
Ce	$5d^1 \rightarrow 4f^1 : {}^2F_{5/2}$	33.333
	${}^2F_{7/2}$	31.348
Pr	$4f^2 : {}^1S_0 \rightarrow {}^3F_4$	40
	${}^1G_4$	37.037
	${}^1D_2$	29.411–29.850
	${}^1I_6$	24.154–25.380
	$4f^2 : {}^3P_0 \rightarrow {}^3H_4$	19.920–20.833
	${}^3H_5$	18.382–18.656
	${}^3H_6$	16.366–16.611
	${}^3F_2$	15.674–15.949
	${}^3F_4$	13.812–14.347
Nd	$5d^1 4f^2 \rightarrow 4f^3 : {}^4I_j$	56.179
	${}^4F_j$	44.643
	${}^4G_j$	39.370
	$4f^3 : {}^4D_{3/2} \rightarrow {}^4I_{9/2}$	28.090
	${}^4I_{11/2}$	26.178
	${}^4I_{13/2}$	24.213
	${}^4I_{15/2}$	22.321
	$4f^3 : {}^4F_{3/2} \rightarrow {}^4I_{9/2}$	11.198–11.560
Sm	$4f^5 : {}^4G_{5/2} \rightarrow {}^6H_{5/2}$	17.825–17.889
	${}^6H_{7/2}$	16.666–16.892
	${}^6H_{9/2}$	15.432–15.674
	${}^6H_{11/2}$	14.084–14.347
	${}^6H_{13/2}$	12.840
Eu	$4f^6 : {}^5D_2 \rightarrow {}^7F_0$	21.552
	${}^7F_1$	21.141–21.231
	${}^7F_2$	20.408–20.576
	${}^7F_3$	19.646
	$4f^6 : {}^5D_1 \rightarrow {}^7F_0$	19.083
	${}^7F_1$	18.621–18.726
	${}^7F_2$	17.605–18.050
	$4f^6 : {}^5D_0 \rightarrow {}^7F_0$	17.182
	${}^7F_1$	16.863–16.949
	${}^7F_2$	15.974–16.286
	${}^7F_4$	14.347–14.556
Gd	$4f^7 : {}^6I_{7/2} \rightarrow {}^8S_{7/2}$	35.971
	$4f^7 : {}^6P_{7/2} \rightarrow {}^8S_{7/2}$	31.847–32.258
	$4f^7 : {}^6G_{7/2} \rightarrow {}^6P_{7/2}$	16.949
	${}^6P_{5/2}$	16.353
	${}^6P_{3/2}$	15.797
	${}^6I_j$	12.804–13.227

(33,333 cm^{-1}) and a shoulder at 319 nm (31 348 cm^{-1}). In view of the lowest $4f$-$5d$ transition (41 666 cm^{-1}) identified in Fig. 1, this gives a Stokes shift of about 8333 cm^{-1}. This relatively large Stokes shift results from an off-center movement of the Ce^{3+} ion after being excited to the $5d$ state, which in turn causes a strong deformation of the tricapped prism of anions around the cerium ion. According to Andriessen *et al.*,[10] it is caused by a reorientation of the occupied states by a pseudo Jahn–Teller coupling to the higher $5d$ states. For NaLaF$_4$:Pr^{3+} an excitation into the $4f^1 5d^1$ levels of Pr^{3+} results at first in a relaxation to the ${}^1S_0$ level and the ${}^1S_0 \rightarrow {}^3F_4$, ${}^1G_4$, ${}^1D_2$, ${}^1I_6$ transitions. A further relaxation from the ${}^1I_6$ state to the ${}^3P_{0,1}$ levels is followed by emission from ${}^3P_0$. The emission lines identified in NaLaF$_4$:Pr^{3+} were found as well in YF$_3$:Pr^{3+}(Ref. 11) at comparable wavelengths. The characteristic $5d$-$4f$ emission of NaLaF$_4$:Nd^{3+} observed in the emission spectrum under $4f^2 5d^1$ excitation was also observed in YPO$_4$:Nd^{3+}, CaF$_2$:Nd^{3+},Na$^+$, and LiYF$_4$:Nd^{3+}.[12] NaLaF$_4$:Sm^{3+} shows under excitation in the $4f^4 5d^1$ levels of Sm^{3+} only ${}^6G_{5/2} \rightarrow {}^6H_J$ ($J=5/2$, $7/2, 9/2, 11/2, 13/2$) transitions. The wavelength region for the different multiplet transitions in NaLaF$_4$:Eu^{3+} does not differ very much from those found in LiYF$_4$:Eu^{3+}.[13,14] After excitation into a $4f^7 : {}^6G_J$ energy level of Gd^{3+} (202 nm), the emission spectrum of NaLaF$_4$:Gd^{3+} reveals emissions in the long wavelength region due to the ${}^6G_{7/2} \rightarrow {}^6P_j$ ($J =3/2, 5/2, 7/2$) and ${}^6G_{7/2} \rightarrow {}^6I_j$ transitions as well as in the UV region due to emissions from both the ${}^6I_{7/2}$ and the ${}^6P_{7/2}$ to the ${}^8S_{7/2}$ GS. The excitation spectra reveal the systematic

behavior of the $5d$ energy states over the Ln series as predicted by the Dorenbos model and will be used to construct the energy level scheme. The emission properties presented here will be used to interpret the TL data that will be presented in the next section.

B. Thermoluminescence

1. Ln monodoped NaLaF$_4$

In Fig. 3 the TL glow curves are plotted wavelength-resolved in a two-dimensional λT-contour plot. It can be seen that the emissions originate from the respective dopant and that the emissions occur mainly, except for NaLaF$_4$:Tb^{3+}, in the low-temperature region between 350 and 500 K. In fact, there are only three cases, NaLaF$_4$:Ln^{3+}

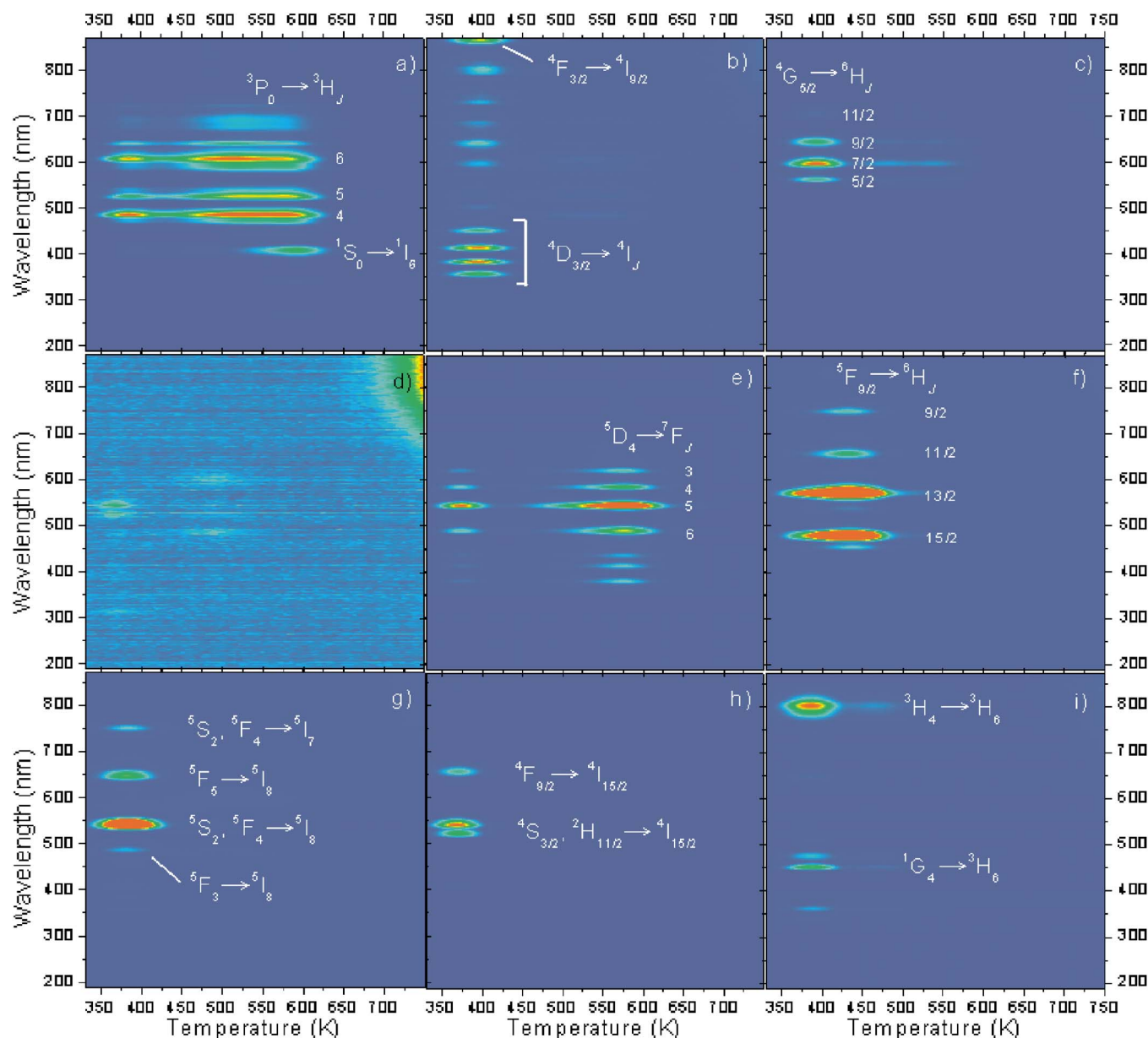FIG. 3. (Color online) λT-contour plots of (a) NaLaF$_4$:Pr^{3+}, (b) NaLaF$_4$:Nd^{3+}, (c) NaLaF$_4$:Sm^{3+}, (d) NaLaF$_4$:Gd^{3+}, (e) NaLaF$_4$:Tb^{3+}, (f) NaLaF$_4$:Dy^{3+}, (g) NaLaF$_4$:Ho^{3+}, (h) NaLaF$_4$:Er^{3+}, and (i) NaLaF$_4$:Tm^{3+} after gamma irradiation of 4 kGy from a ^{60}Co source; heating rate=5 K/s.

(Ln=Ce, Pr, Tb), for which an additional band appears around 570 K. We refer to the first band between 350 and 500 K as C1 and the second band around 570 K as C2 for those three cases [Fig. 4(a)]. The C1-band is composed of two glow peaks. Figure 4(b) shows the normalized glow peaks of NaLaF$_4$:Ln^{3+} (Ln=Nd, Dy, Er, Tm), which feature only one TL-band at lower temperatures and no emission at higher temperatures. We call this low temperature TL-band C3. Unlike the C1-band, the position of the C3-band depends on the type of Ln dopant. The particular temperature of maximum luminescence intensity increases in the order Er <Tm<Nd<Dy. For NaLaF$_4$:Ln^{3+} (Ln=Sm, Eu, Gd, Yb), either no TL at all (Eu, Yb) or only very weak TL (Sm, Gd) was found. We can summarize that the Ln monodoped NaLaF$_4$ samples can be divided into three groups, viz., samples with Ln dopants which show (1) two bands C1 and C2, (2) only one band C3, or (3) no TL emission at all.

2. Ce–Ln codoped NaLaF$_4$ and NaLaF$_4$:2% Ce^{3+}

For all Ce–Ln codoped NaLaF$_4$ samples, mainly the $5d$-$4f$ emission of cerium is observed (Fig. 5). The λT-contour plot in Fig. 5(c) is very noisy as the detection sensitivity of the CCD camera was too low for the very weak emission of NaLaF$_4$:Ce^{3+}, Sm^{3+}; nevertheless, a faint spot around 320 nm can be identified. The normalized glow curves for NaLaF$_4$:Ce^{3+}, Ln^{3+} (Ln=Sm, Er, Tm) and NaLaF$_4$:Ce^{3+} are shown in Fig. 6. They all show a band between 350 and 450 K, which is composed of two glow peaks and will also be referred to as C1 as in the case of NaLaF$_4$:Ln^{3+} (Ln=Ce, Pr, Tb). Additionally, to the C1-band, Fig. 6 reveals a second band with its temperature for maximum luminescence intensity varying between 470 and 800 K. This band was not observed before and will be called C4 for all Ce–Ln codoped NaLaF$_4$ samples. The temperature for
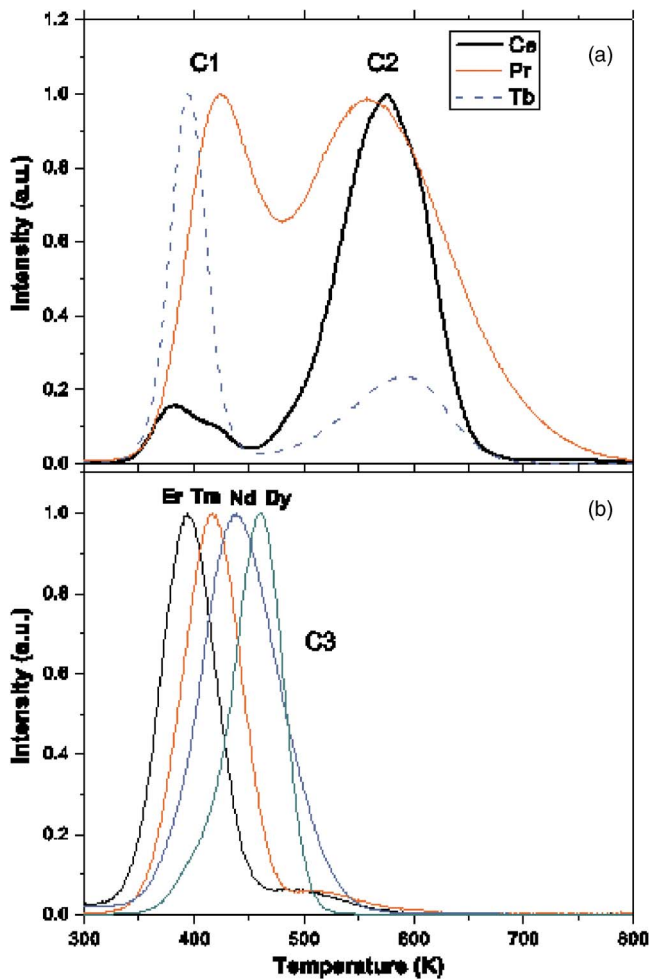
FIG. 4. (Color online) Normalized glow curves of (a) NaLaF$_4$:Ln^{3+} (Ln =Ce,Pr,Tb) and (b) NaLaF$_4$:Ln^{3+} (Ln=Nd,Dy,Er,Tm) after beta irradiation of 1280 mGy, recorded with a heating rate of 5 K/s.

maximum intensity of C4 increases in the order Ce,Ho <Ce,Tm<Ce,Sm (see Fig. 6). This behavior was also observed in YPO$_4$:Ce^{3+}, Ln^{2+}(Ref. 15) and Ca$_2$MgSi$_2$O$_7$:Eu^{2+},Ln^{3+}.[16]

IV. DISCUSSION

A. Photoluminescence and energy level diagram

1. Ln^{2+} 4f GSE location

The band around 119 nm in the excitation spectra (Fig. 1, left hand) is assigned to exciton creation. The second band around 108 nm (11.5 eV) in NaLaF$_4$:Ce^{3+} has been identified by us as the band gap. In the case of NaLaF$_4$:Eu^{3+}, the fluoride-europium CT band $E^{CT}(6,3+,A)$ can be clearly seen at about 160 nm, thus setting the $^8S_{7/2}$ GS of Eu^{2+} (4f^7) approximately 7.7 eV above the top of the VB. The location of the 4f^{n+1} GSs of all other divalent lanthanides can now be obtained using[1]

$$E_{Vf}(n+1,2+,A) = E^{CT}(6,3+,A) + \Delta E_{Vf}(n+1,7,2+),$$

(1)

where $E_{Vf}(n+1,2+,A)$ is the energy difference between the top of the VB of a compound A and the 4f^{n+1} GSE of a

divalent Ln dopant ion and $\Delta E_{Vf}(n+1,7,2+)$ denotes the average energy difference between that ion and the 4f^7:$^8S_{7/2}$ energy level of Eu^{2+}. The values for $\Delta E_{Vf}(n+1,7,2+)$ are known.[17] The 4f GSEs for the divalent Ln dopant ions obtained in this way are shown, relative to the VB and the CB of NaLaF$_4$, in Fig. 7.

2. Ln^{3+} 4f GSE location

The positioning of the 4f GSEs for the trivalent lanthanides is trickier than that for the divalent dopant ions as we do not observe any CT band to tetravalent Ln ions, and we have no experimental indications of 5d energy level locations relative to the electronic host states. However, we have indications that in wide band gap compounds like fluorides, the energy difference between the 4f^6 GSE of Eu^{3+} and the 4f^7 GSE of Eu^{2+} is between 6.6 and 7.3 eV.[17,18] We also found that for Ln monodoped NaLaF$_4$, four samples, viz., NaLaF$_4$:Ln^{3+} (Ln=Sm,Eu,Gd,Yb), either do not show glow peaks at all or at least, as for NaLaF$_4$:Sm^{3+} and NaLaF$_4$:Gd^{3+}, show only very weak emission. It will be explained in the next section that the presence of glow peaks with emission from the Ln dope additive requires the 4f^n GSE being sufficiently above the VB. Keeping this in mind, we can conclude that for Sm, Eu, Gd, and Yb, the 4f^n GSs must lie either quite close to the VB or even inside it. We will adopt the 6.7 eV for the Eu^{3+}/Eu^{2+} energy difference mentioned above. The $^8S_{7/2}$ GS of Gd^{3+} is then energetically placed just below the top of the VB (see Fig. 7). Using the average energy difference between the GSE of a trivalent Ln ion and the $^8S_{7/2}$ GSE of Gd^{3+} given in Ref. 17, we can now place the 4f^n GSEs of all other trivalent Ln ions. In so doing, we get a complete energy level diagram for NaLaF$_4$, which is shown in Fig. 7.

B. Electron- and hole-traps

Under MeV energy beta or gamma irradiation, many electrons will be raised from the VB to the CB. Now, apart from relaxing back to the VB in order to recombine with the holes left behind, the excited electrons may be trapped either by host defects or the lanthanide impurities. Trivalent lanthanides can trap electrons (Ln^{3+}+e^-→Ln^{2+}) when their 4f GSE in the divalent form is located below the CB. As can be seen in Fig. 7, this holds for all lanthanides other than La, Ce, and Gd. The holes, in contrast, polarize the lattice and either form self-trapped holes (V_k-centers) or are trapped by Ln dopants (Ln^{3+}+h→Ln^{4+}). When a V_k-center is formed, it can be stabilized in turn by a lattice defect or a Ln impurity.[19,20] Below, a V_k-center stabilized by a defect will be termed V_{kA}-center. A V_{kA}-center-release means the liberation of the V_K-center from that defect. Only if the 4f GSE of the lanthanide dopant (relative to the VB) is located above the V_{kA}-center energy E_A, the hole can be trapped in the 4f state of the lanthanide. The energy of V_k-centers is not affected very much by different fluoride host lattices,[21] and the difference between the VB and the GSE of the V_k-center is known to be in the order of few eV.[22,23]
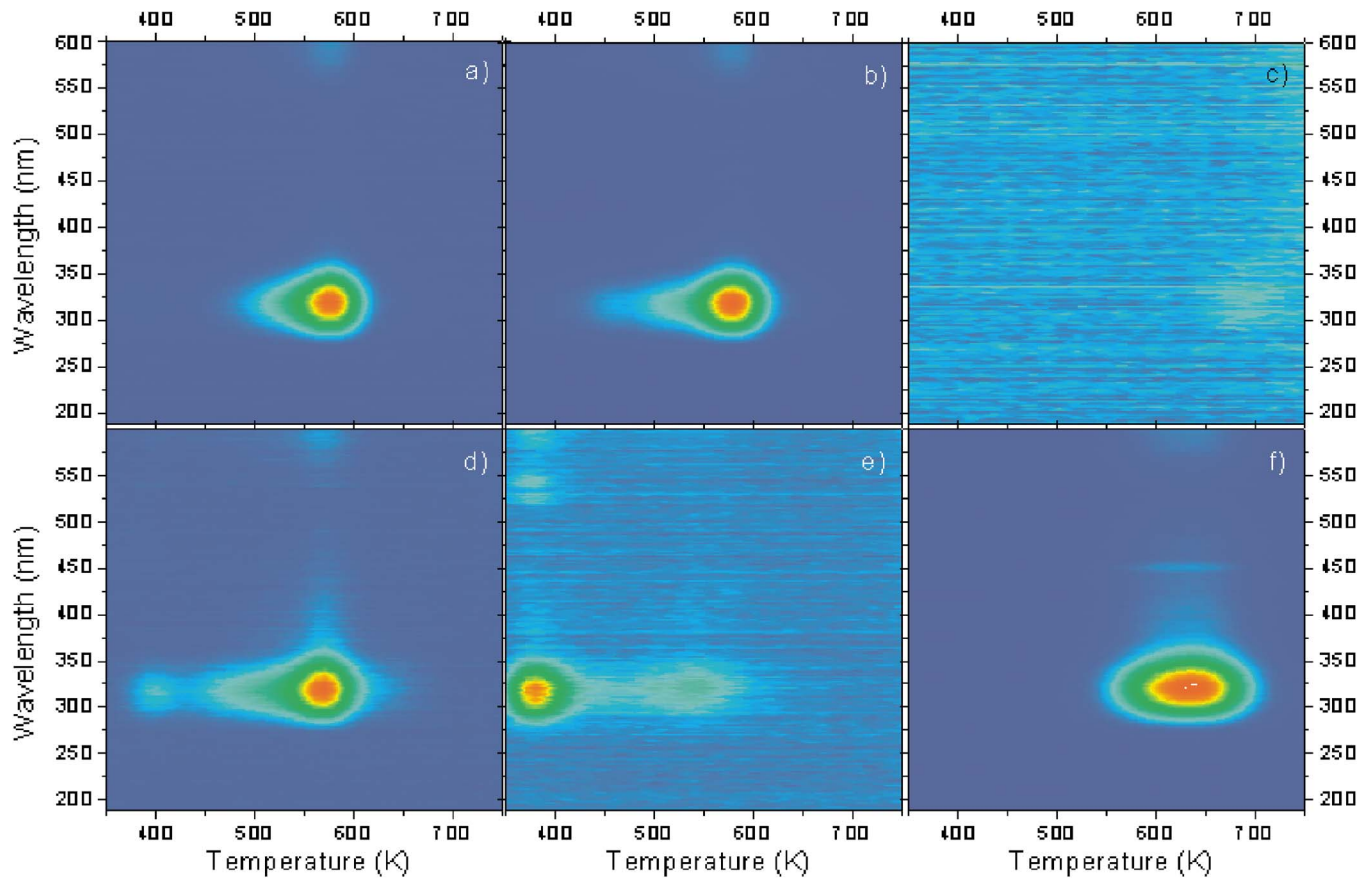
FIG. 5. (Color online) λT-contour plots of (a) $NaLaF_4:Ce^{3+}$, (b) $NaLaF_4:Ce^{3+}, Nd^{3+}$, (c) $NaLaF_4:Ce^{3+}, Sm^{3+}$, (d) $NaLaF_4:Ce^{3+}, Ho^{3+}$, (e) $NaLaF_4:Ce^{3+}, Er^{3+}$, and (f) $NaLaF_4:Ce^{3+}, Tm^{3+}$ after gamma irradiation of 4 kGy from a ^{60}Co source; heating rate=5 K/s.

C. Thermoluminescence

Based on the possible electron- and hole-traps described in Sec. IV B, we can now construct a model which is able to explain the observed TL properties of each sample. This can be done by assuming only two host related electron traps with activation energies E1 and E2. With it, two principal processes are thinkable leading to the observed glow peaks, viz., (1) an electron being released from an E1- or E2-trap or a Ln^{2+} impurity, recombining with a hole trapped at a trivalent Ln dopant and (2) a thermal liberation and transfer by hopping of either the V_{kA}-center or the Ln-trapped hole with subsequent recombination with a divalent Ln ion forming an excited state of Ln^{3+}. The decay of this excited state results
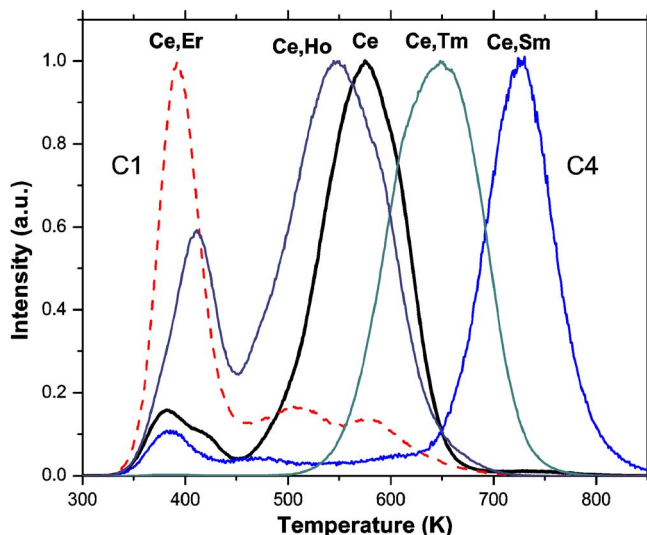

FIG. 6. (Color online) Normalized glow curves of $NaLaF_4:Ce^{3+}$ and $NaLaF_4:Ce^{3+}, Ln^{3+}$ (Ln=Sm,Ho,Er,Tm) after beta irradiation of 1280 mGy, recorded with a heat rate of 5 K/s.
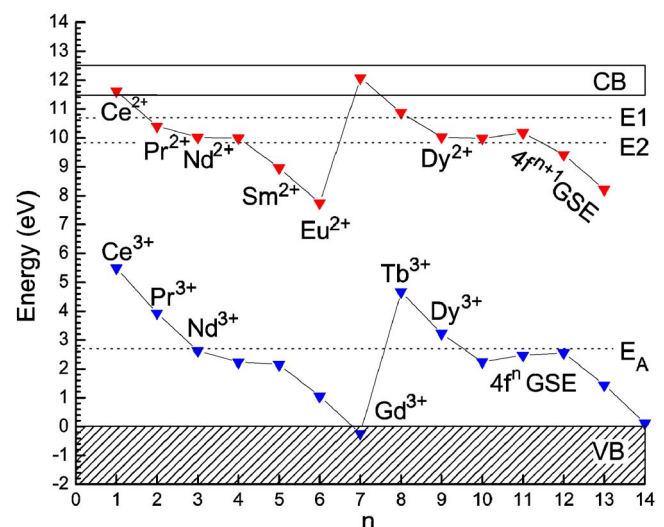

FIG. 7. (Color online) Energy level scheme for $NaLaF_4:Ln^{3+}$ showing the Ln^{2+} ($4f^{n+1}$) and Ln^{3+} ($4f^n$) GSs. The activation energies E1, E2, and the V_{kA}-center energy E_A are indicated by dashed lines.

TABLE II. Relative luminescence intensity I_{rel}, activation energy E (eV), natural logarithm of the frequency factor s, and glow peak maximum T_m (K) in K for the C4-band in Ce–Ln codoped NaLaF$_4$.

Dopants	$I_{rel}(C4)$	$T_m(C4)$	$E(C4)$	$\ln(s)$
Ce, Nd	0.99	601	⋯	⋯
Ce, Sm	0.05	726	1.48	19.49
Ce, Dy	0.48	590	⋯	⋯
Ce, Ho	0.29	543	⋯	⋯
Ce, Er	0.21	⋯	⋯	⋯
Ce, Tm	1	646	1.42	22.21
Ce, Yb	0	⋯	⋯	⋯

in TL with an emission spectrum characteristic for the Ln^{3+} ion. Recombination of a released hole with an electron in E1- or E2-traps is, in principle, possible. If it occurs, it is a non-radiative recombination.

1. Activation energy

The activation energies for both the electron- and hole-traps were obtained assuming first-order kinetics, i.e., neglecting retrapping during heating. In this case, the condition for the maximum TL intensity can be written as an Arrhenius equation[24]

$$\ln(T_m^2/\beta) = E/k_B T_m + \ln(E/k_B s), \qquad (2)$$

where β is the heating rate (in K/s), E the activation energy or trap depth, k_B the Boltzmann constant, s the frequency factor (in s^{-1}), and T_m the temperature for which the luminescence intensity is maximal. Plotting Eq. (2) against $1/k_B T_m$ (heating rate plots) results in a straight line with slope E and an intercept of $\ln(E/s \cdot k_B)$. In Fig. 8 both the glow curves for different heating rates and the heating rate plot are shown for NaLaF$_4$:Dy^{3+}. It can be seen that the luminescence intensity decreases with decreasing β. This behavior was also observed in all other samples except for NaLaF$_4$:Nd^{3+}. We have observed this behavior earlier in YPO$_4$:Ce^{3+}, Sm^{3+} and explained it by fading before and dur-

ing readout due to center-to-center recombination of electrons trapped by Sm^{3+} with holes on the Ce^{3+} site.[15] The fact that the points in the heating rate plot YPO$_4$:Ce^{3+} indicate a slightly parabolic behavior rather than a straight line may be caused by a temperature gradient between the heating element and the sample surface.[25]

2. Ce–Ln codoped NaLaF$_4$

In the case of Ce–Ln codoped NaLaF$_4$, it was noticed earlier that all TL was mainly due to $5d$-$4f$ cerium emission (see Fig. 5). The energy level diagram (Fig. 7) shows that the GSE of divalent cerium is above the CB, whereas the GS of trivalent cerium is located inside the band gap, well above the VB. Ce^{3+} is therefore a very stable hole-trap (Ce^{3+}+h →Ce^{4+}). It suggests that the only possibility for charge carrier recombination is an electron recombining with tetravalent cerium leaving an excited state of cerium in the trivalent form Ce^{4+}+e^-→(Ce^{3+})*. It now comes to finding the origin of the electron. The TL curves of all Ce–Ln codoped samples show two bands, viz., C1 and C4. The C1-band is composed of two glow peaks and situated at the same temperature for all types of Ln^{3+} codopants. This indicates that it is due to an electron-release from a host related E1-trap. The C4-band, in contrast, varies with the Ln^{3+} codopant (see Fig. 6). As the $4f^{n+1}$ GSEs of all divalent Ln ions in question are located below the CB, it is obvious to explain the Ln-specific C4-band by an electron-release from those dopants: Ln^{2+} →Ln^{3+}+e^-. Thus, the order of the different C4-bands shown in Fig. 6 reflects a trend in the energy difference between the $4f^{n+1}$ GSE and the CB as expected from the Dorenbos model and shown in Fig. 7. Now, aside from NaLaF$_4$:Ce^{3+}, Sm^{3+} and NaLaF$_4$:Ce^{3+}, Tm^{3+}, the C4-band is located between 470 and 650 K in all Ce–Ln codoped NaLaF$_4$ cases, overlapping strongly with the corresponding band (C2) in NaLaF$_4$:Ce^{3+}. Looking at Fig. 7 we see that the $4f$ GS of Ce^{2+} is located inside the CB. Since the C2-band in NaLaF$_4$:Ce^{3+} must therefore be due to an electron-release from a host related E2-trap, we have to assume a contribution of the E2-trap also in NaLaF$_4$:Ce^{3+}, Ln^{3+}. In most cases, the C4-band is composed of an undefined number of glow
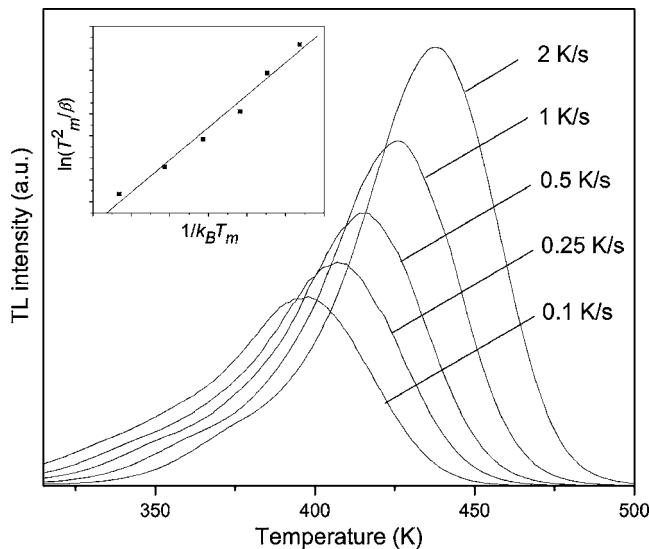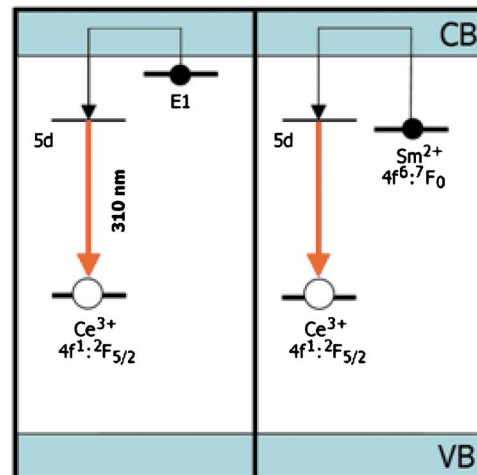

FIG. 8. Glow curves for NaLaF$_4$:Dy^{3+} for different heating rates after a dose of 1280 mGy; the inset shows corresponding heating rate plot.

FIG. 9. (Color online) Model explaining the origin of the glow curves for NaLaF$_4$:Ce^{3+}, Sm^{3+}.

TABLE III. Relative luminescence intensity I_{rel}, temperature for maximum luminescence intensity T_m (K), activation energy E (eV), natural logarithm of the frequency factor s, and the frequency factor relative to Dy, s_{rel}, for the C3-band in Ln monodoped NaLaF$_4$.

Dopant	$I_{rel}(C3)$	$T_m(C3)$	$E(C3)$	$\ln(s)$	s_{rel}
Ce	$\cdots$	378	0.74	$\cdots$	$\cdots$
Pr	0.05	419	0.71	19.36	0.001
Nd	0.07	438	0.75	19.10	0.001
Sm	0.0001	464	0.71	18.88	0.0007
Gd	0.001	401	0.68	19.08	0.001
Tb	0.1	392	0.76	22.37	0.02
Dy	1	460	1.06	26.20	1
Ho	0.01	403	0.76	21.73	0.01
Er	0.01	394	0.73	20.95	0.01
Tm	0.02	416	0.72	19.33	0.001

peaks. Peak separation was only possible for NaLaF$_4$:Sm^{3+} and NaLaF$_4$:Tm^{3+}. Additionally, their C4-bands are at perspicuously higher temperatures compared to all other Ce–Ln codoped NaLaF$_4$ samples, and therefore, in these two cases, we attribute the C4-band to an electron-release from the respective divalent $4f^{n+1}$ GS.

Table II contains the activation energies derived from C4 for those two samples and information about the relative luminescence intensity I_{rel} and T_m of all investigated codoped samples. The $4f^{n+1}$ GSEs of Sm^{2+} and Tm^{2+} found via glow peak analysis (see Table II) are about 0.96 and 0.56 eV, respectively, closer to the CB than the ones obtained from the fluoride-europium CT band and the Dorenbos model (Fig. 7). One reason for this difference might be that the C4-bands for NaLaF$_4$:Ce^{3+}, Sm^{3+} and NaLaF$_4$:Ce^{3+}, Tm^{3+} could still be composed of more than one peak, making it difficult to establish the right T_m value. Another reason could be a wrong assignment of the band gap in the excitation spectra of NaLaF$_4$:Ln^{3+} (see Sec. III, Fig. 1). The notable differences in luminescence intensities are not understood yet. In general, the luminescence intensities of the codoped samples are about half as intensive as the ones of the monodoped samples.

In Fig. 9 the main recombination process for the codoped samples is depicted exemplary for NaLaF$_4$:Sm^{3+}. The C1-band is due to an electron-release from the E1-trap (Fig. 9, left part), whereas the C4-band originates from an electron-release from the rather deep lying $4f$ GSE of divalent samarium (Fig. 9, right). The contribution from the E2-trap is missing. This might indicate that Sm ions trap electrons more efficiently than host related electron traps or that the electrons from E2-traps relax to the $^7F_0$ GS of Sm^{2+}.

3. Ln monodoped NaLaF$_4$

For NaLaF$_4$:Ln^{3+} we found that the TL was due to $4f$-$4f$ emission of the Ln^{3+} dope additive (see Fig. 3). So, in principle, we can think of two different charge carrier recombination processes: (1) an electron recombines with a Ln-trapped hole giving an excited $4f$ state of Ln^{3+}:Ln$^{4+}+e^- \rightarrow$(Ln^{3+})* and (2) a hole recombines with a Ln-trapped electron resulting in an excited $4f$ state of Ln^{3+}:Ln$^{2+}+h \rightarrow$(Ln^{3+})*. Now it comes to asking about the origin of either an electron or a hole. We know that only NaLaF$_4$:Ln^{3+} (Ln

=Ce, Pr, Tb), whose Ln dopants $4f^n$ GSs are deep hole-traps, shows two glow bands, C1 and C2 [Fig. 4(a)]. All other monodoped samples feature solely the C3-bands [Fig. 4(b)]. For explaining the two TL bands in NaLaF$_4$:Ln^{3+} (Ln =Ce, Pr, Tb), we can use the same argument as in the last section, that is, the assumption of (1) an electron-release from an E1-trap for explaining the C1-band and (2) an electron-release exclusively from an E2-trap (Ce) or together with an electron-release from a divalent Ln ion (Pr, Tb), in order to explain the C2-band. The other Ln monodoped NaLaF$_4$ cases show only the C3-band, as already mentioned. In Table III the activation energies $E(C3)$ for the C3-band are shown. Apart from Dy^{3+}, they are almost the same for all dopants with an average of 0.73 eV. As dysprosium has a higher activation energy than all the other Ln dopants, the C3-band cannot be due to an electron-release neither from a host related E1-trap nor from the divalent Ln dopant ions. The $4f^{n+1}$ GSEs of the latter are not so different from the one of dysprosium so that in the case of an electron-release from the Ln^{2+} ions, we would expect similar activation energies for all of these dopants (see Fig. 7). Thus, we deal with a hole-release as the only remaining possibility. The 0.73 eV
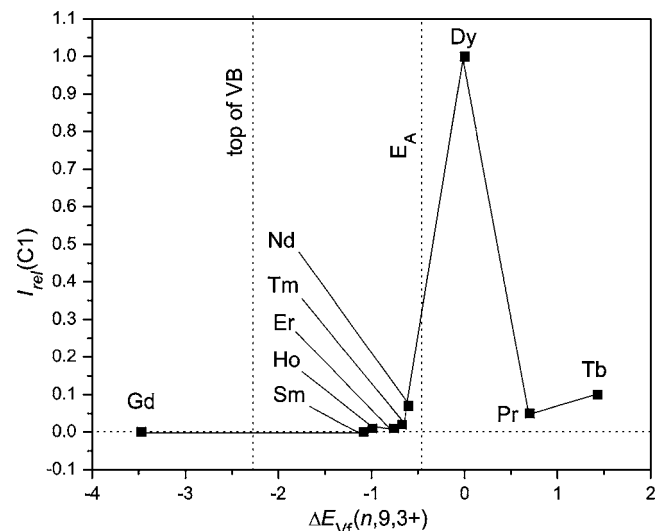

FIG. 10. Relative luminescence intensity $I_{rel}(C1)$ vs $\Delta E_{Vf}(n,9,3+)$ in NaLaF$_4$:Ln^{3+}. Ln is specified inside the figure. Top of VB and lattice defect energy E_A relative to the VB are indicated by dotted vertical lines.
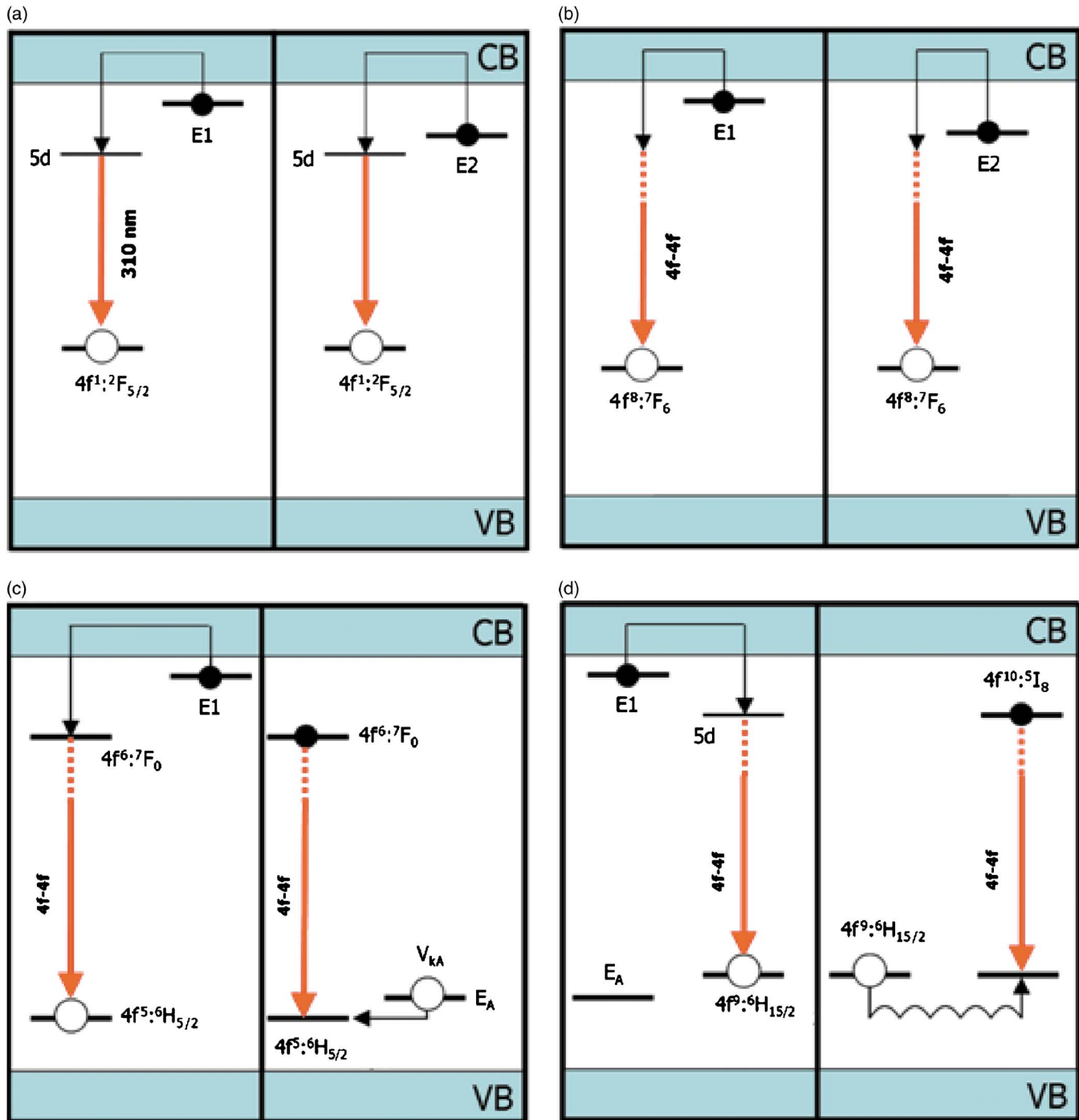
FIG. 11. (Color online) Model explaining the origin of the glow curves for (a) $NaLaF_4:Ce^{3+}$, (b) $NaLaF_4:Tb^{3+}$, (c) $NaLaF_4:Sm^{3+}$, and (d) $NaLaF_4:Dy^{3+}$.

activation energy of the C3-band is assumed to be the total energy needed to thermally free a V_{kA}-center and transfer the hole via a hopping mechanism to the GS of a divalent Ln dopant. Dy^{3+}, in contrast, not only features its glow peak at the relative highest temperature (460 K) but shows also the most intense TL among all dopants. We assume the corresponding activation energy of 1.06 ± 0.04 eV in this case not to indicate a V_{kA}-center-release but a hole-release from dysprosium together with hole transfer by hopping. The reason for this assumption is the relative large energy difference between the top of the VB and the $^6H_{15/2}$ Dy^3 state compared to all other Ln ions except for Ce, Pr, and Tb. The 4f GSEs

of those three latter ions are located so high above the VB that the energy needed to free the hole exceeds the activation energies E1 and E2 so that in this case recombination with ensuing luminescence will be achieved by electron-release via the CB. The GSE of the V_{kA}-center, E_A, must be located between the Dy^{3+} and the Ho^{3+}, Er^{3+} and Tm^{3+} 4f GS at about 2.7 eV above the top of the VB; it is indicated in Fig. 7 as a dotted line. This value is very realistic for V_{kA}-centers in fluorides.

In order to explain the origin of the Ln-specific glow peaks, Raymond *et al.*[17] and Yang *et al.*[18] analyzed the relation between T_m and the ionic radii of the lanthanides. Here

we want to turn the attention to the relation between the relative luminescence intensity I_{rel} and the average energy difference between the $^6H_{11/2}$ GSE of dysprosium and the $4f$ GSEs of the other trivalent Ln ions, $\Delta E_{Vf}(n,9,3+)$ (depicted in Fig. 10). It can be clearly seen that the luminescence intensity does not only depend on the location of the $4f^n$ GS relative to the top of the VB but also to the presumable location of the V_{kA}-center GSE. The high luminescence intensity in NaLaF$_4$:Dy^{3+} might indicate a higher hole trapping efficiency of lanthanides than of V_K-centers once the Ln^{3+} $4f^n$ GSE is located above the V_{kA}-center energy. By comparing column two with column six of Table III, a correlation of the luminescence intensity with the frequency factor can be seen. The Ln-specific frequency factor correlates also roughly with the temperature for the highest TL intensity of the C3-band [see Fig. 4(b)]. In Fig. 11 our model is further illustrated, explaining the conjectured internal processes leading to the glow curves of NaLaF$_4$:Ln^{3+} (Ln =Ce,Tb,Sm,Dy). Both for NaLaF$_4$:Ce^{3+} and NaLaF$_4$:Tb^{3+}, the two glow bands labeled above C1 and C2 can be seen in [Fig. 4(a)]. Within the model, those two bands are due to the two different electron E1- and E2-traps, respectively. Being thermally released from the traps, the electrons excite in NaLaF$_4$:Ce^{3+} via the CB, the Ce^{3+} ions resulting in the characteristic $5d$-$4f$ emission [see Fig. 11(a)]. In NaLaF$_4$:Tb^{3+} the Tb^{2+} $4f^9$:$^6H_{15/2}$ GS may additionally act as an electron-trap as it lies below the CB, though closer to it than E1 and E2 [see Fig. 11(b), left part]. Now, besides Ce, Pr, and Tb, all other Ln monodoped samples feature (if at all) only the C3-band while having no band at higher temperatures. In Figs. 11(c) and 11(d) this is exemplified for NaLaF$_4$:Sm^{3+} and NaLaF$_4$:Dy^{3+}. Their $4f^{n+1}$ GSs, $4f^6$:$^7F_0$ (Sm^{2+}) and $4f^{10}$:$^5I_8$ (Dy^{2+}), respectively, both lie energetically below the CB thus being able to trap electrons. In addition their $4f^n$ GSEs are located closer to the VB than the ones of Ce, Pr, and Tb so that in these cases a hole-release must also be considered, either via the liberation of the V_{kA}-center as in the case of Sm^{3+} [Fig. 11(c)] or from the Ln dopant itself as in the case of Dy^{3+} [Fig. 11(d)]. After being released from Dy^{3+}, the hole will be trapped in the form of a V_k-center, which then is transferred by hopping to a Dy^{2+} ion. The type of release depends on the locations of the $4f$ GSs relative to the V_{kA}-center GSE. The same holds for all other Ln ions except Eu, Gd, and Yb as their $4f$ GSs are located too close to or even inside the VB. The reason why no TL was found in NaLaF$_4$:Eu^{3+} could be due to fading between the V_{kA}-center GSE, E_A, and the GSE of Eu^{2+}. The activation energies E1 and E_A appear to be of similar magnitude so that both corresponding traps contribute to the glow band called C3. Therefore, it is not always possible to separate them.

V. CONCLUSION

Based on PL-, TL-spectra, and information from literature about the energy difference between the $4f^6$ GSE of Eu^{3+} and the $4f^7$ GSE of Eu^{2+} in wide band gap compounds, a complete energy level diagram for NaLaF$_4$:Ln^{3+} was con-

structed. This diagram motivated TL measurements on Ln mono- and Ce–Ln codoped NaLaF$_4$. In the Ln monodoped NaLaF$_4$ case, we found that the TL was due to $4f$-$4f$ emission from the Ln^{3+} dopant ion. NaLaF$_4$:Ln^{3+} (Ln =Ce,Pr,Tb) shows two TL-bands, whereas NaLaF$_4$:Ln^{3+} (Ln=Nd,Dy,Ho,Er) features only one TL-band. NaLaF$_4$:Ln^{3+} (Eu, Gd, and Yb) shows either no or very weak TL. In Ce–Ln codoped NaLaF$_4$, the TL emission was mainly due to $5d$-$4f$ emission from Ce^{3+}. It was shown that in addition to the energy level diagram, only two assumptions, viz., the presence of two host related electron traps and the presence of V_k-centers, are necessary for explaining the Ln-specific glow peaks. Thus, we can conclude that (1) a Ln ion can serve as an electron trap only when its Ln^{2+} $4f^{n+1}$ GSE is located below or close to the activation energies of the host related E1- and E2-electron traps relative to the CB and (2) a Ln ion can serve as a hole-trap only when its Ln^{3+} $4f^n$ GSE is located above the V_{kA}-center GSE, E_A, relative to the VB.

[1] P. Dorenbos, J. Lumin. **108**, 301 (2004).
[2] E. van der Kolk, Chem. Mater. **18**, 3458 (2006).
[3] V. A. Gubanov and M. V. Ryzhkov, J. Struct. Chem. **27**, 781 (1987).
[4] A. Meijerink, W. J. Schipper, and G. Blasse, J. Phys. D **24**, 997 (1991).
[5] D. Meiss, W. Wischert, and S. Kemmler-Sack, Mater. Chem. Phys. **38**, 191 (1994).
[6] A. Aebischer, M. Hostettler, J. Hauser, K. W. Krämer, T. Weber, H. U. Güdel, and H. B. Bürgi, Angew. Chem., Int. Ed. **45**, 2802 (2006).
[7] K. W. Krämer, D. Biner, G. Frei, H. U. Güdel, M. P. Hehlen, and S. R. Lüthi, Chem. Mater. **16**, 1244 (2004).
[8] W. H. Zachariasen, Acta Crystallogr. **1**, 265 (1948).
[9] P. Dorenbos, Phys. Rev. B **62**, 15640 (2000).
[10] J. Andriessen, E. van der Kolk, and P. Dorenbos, Phys. Rev. B **76**, 075124 (2007).
[11] S. Kück, I. Sokólska, M. Henke, and E. Osiac, Chem. Phys. **310**, 139 (2005).
[12] L. van Pieterson, Ph.D thesis, Proefschrift Universiteit Utrecht, 2001.
[13] C. Görller-Walrand and M. Behets, Inorg. Chim. Acta **109**, 83 (1985).
[14] B. Bihari, K. K. Sharma, and L. E. Erickson, J. Phys.: Condens. Matter **2**, 5703 (1990).
[15] P. Dorenbos and A. J. J. Bos, Radiat. Meas. (to be published).
[16] T. Aitasalo, J. Hölsä, M. Kirm, T. Laamanen, M. Lastusaari, J. Niittykoski, J. Raud, and R. Valtonen, Radiat. Meas. **42**, 644 (2007).
[17] P. Dorenbos, J. Phys.: Condens. Matter **15**, 8417 (2003).
[18] P. Dorenbos and E. van der Kolk, Appl. Phys. Lett. **89**, 061122 (2006).
[19] S. G. Raymond, B. J. Luff, P. D. Townsend, X. Feng, and G. Hu, Radiat. Meas. **23**, 195 (1994).
[20] B. Yang, P. D. Townsend, and A. P. Rowlands, Phys. Rev. B **57**, 178 (1998).
[21] F. W. Patten and M. J. Marrone, Phys. Rev. **142**, 513 (1966).
[22] A. Norman Jette, T. L. Gilbert, and T. P. Das, Phys. Rev. **184**, 844 (1969).
[23] A. M. Stoneham, *Theory of Defects in Solids: Electronic Structure of Defects in Insulators and Semiconductors* (Oxford University Press, New York, 2001).
[24] R. Chen and S. W. S. McKeever, *Theory of Thermoluminescence and Related Phenomena* (World Scientific, Singapore, 1997).
[25] T. M. Piters and A. J. J. Bos, J. Phys. D **27**, 1747 (1994).